

# Interfacial phenomena in thermally sprayed multiwalled carbon nanotube reinforced aluminum nanocomposite

T. Laha<sup>a</sup>, S. Kuchibhatla<sup>b</sup>, S. Seal<sup>b</sup>, W. Li<sup>c</sup>, A. Agarwal<sup>a,\*</sup>

<sup>a</sup> Mechanical and Materials Engineering, Florida International University, 10555 West Flagler Street, EC 3464, Miami, FL 33174, USA

<sup>b</sup> AMPAC, Nanoscience and Technology Center (NSTC) and Mechanical, Materials and Aerospace Engineering, University of Central Florida, Orlando, FL, USA

<sup>c</sup> Department of Physics, Florida International University, Miami, FL, USA

Received 17 July 2006; accepted 14 September 2006

Available online 4 December 2006

## Abstract

The interfacial phenomena in thermally sprayed (plasma and high-velocity oxyfuel spraying) hypereutectic Al–Si composite with multiwalled carbon nanotube (MWCNT) reinforcement have been analyzed both theoretically and experimentally. The formation of an ultrathin  $\beta$ -SiC reaction layer at the interface is confirmed. Plasma sprayed composite exhibits a thicker SiC layer ( $\sim 5$  nm) than the high-velocity oxyfuel sprayed composite ( $\sim 2$  nm). The presence of SiC layer formation is also corroborated in a chemical vapor deposition experiment where Si was deposited on MWCNTs. The formation of  $\beta$ -SiC is responsible for the improved wettability of the molten Al–Si alloy matrix with MWCNT reinforcement.

© 2006 Acta Materialia Inc. Published by Elsevier Ltd. All rights reserved.

**Keywords:** Metal matrix composite (MMC); Aluminum alloy; Multiwalled carbon nanotube; Thermal spraying; interfacial wetting

## 1. Introduction

Carbon nanotube (CNT) reinforcement has recently been used in the field of composite materials, as this technique offers unique mechanical, electrical and thermal properties [1–7]. A great deal of research on CNT-reinforced composites has focused on synthesizing polymer matrix composites (PMCs) with the aim of improving their mechanical, thermal and electrical properties [8–16]. There has been comparatively little research on synthesizing Al, Mg, Ti, Cu, Ni and Co based metal matrix composites (MMCs) reinforced with CNTs [17–24]. Major challenges in the synthesis of CNT-reinforced MMCs include the difficulty of incorporating and distributing evenly CNTs in the matrix. Successful fabrication of multiwalled carbon nanotube (MWCNT)-reinforced hypereutectic Al–Si composite

using thermal spray forming (plasma spray and high-velocity oxyfuel (HVOF) spray) has been demonstrated by our research group [25,26]. Both retention and homogeneous macroscale distribution of MWCNTs throughout the Al–Si matrix was observed [26].

In addition to studying retention and dispersion of CNTs in MMCs, the interface between the CNTs and the metal matrix needs further attention. The structural strength of the composite material greatly depends on the chemistry, atomic structure and the bonding at the interface, as the mechanical load transfer from the matrix to higher strength reinforcement occurs only through the interface [8,27–29]. The metal matrix should possess good wettability with the reinforcing material in order to avoid microscale cavity formation and ensure good adherence at the interface to avoid any delamination at the interface [29–33]. The wettability, which is determined by the contact angle in solid–liquid systems, depends on several factors, including the surface tension of liquid/molten matrix, the

\* Corresponding author. Tel.: +1 305 348 1701; fax: +1 305 348 1932.  
E-mail address: [agarwala@fiu.edu](mailto:agarwala@fiu.edu) (A. Agarwal).

surface properties of the reinforcement and processing parameters, i.e. temperature, pressure and atmosphere [28–33]. Furthermore, the formation of the reaction product at the interface plays a major role in altering the wetting characteristics [23–35].

Interfacial bonding in polymer matrix composites (PMCs) has been investigated by a number of researchers [8,29,36–40]. Repeated stirring and solution evaporation with high-energy sonication of CNT–polymer mixtures causes mechanical interlocking between the CNTs and the polymer matrix [36,37]. Both covalent and non-covalent bonding between the CNT–polymer matrix can be induced by creating surface defects on CNTs by acid treatment and functionalization [38–40].

Very few studies have documented any improvement in interfacial bonding by enhancing the wettability in CNT–MMCs. Carreno-Morelli et al. employed Mg-coated MWCNTs to synthesize a Mg–MMC with good adherence by successive hot pressing and hot isostatic pressing. An ultrathin layer ( $\sim 5$  nm) of Mg coating on MWCNTs was formed by solvent treatment of the CNTs, after surface modification by sodium dodecyl sulfate [19]. In synthesizing Cu–MWCNT composite by powder metallurgy, improvement in the wettability was achieved using Ni-coated MWCNTs [21,23]. In a Co–MWCNT composite, synthesized by an electroless process, MWCNTs with surfaces etched by an acidic  $\text{CrO}_3$  solution were used to improve the interfacial bonding [24]. However, the important factors controlling wetting kinetics (i.e. the change in wetting angle with time) – namely the effect of (i) atomic structure in the MWCNTs, (ii) alloying elements in the liquid matrix, (iii) interfacial reaction occurring, if any, and (iv) processing conditions, i.e. temperature and atmosphere – remain unexplored in CNT–MMCs.

The goal of the present work was to study the interface between the hypereutectic Al–Si alloy matrix and the MWCNT reinforcement in composites synthesized by plasma spraying and HVOF spraying techniques. The wetting behavior and the interface between the Al–Si alloy and the MWCNTs have been investigated. The role of Si as alloying element and the severe processing conditions (i.e.

thermal spraying at very high temperature and velocity) are further elucidated to improve the wetting kinetics.

## 2. Materials and methods

### 2.1. Composite fabrication using thermal spray forming

Gas atomized, prealloyed, spherical hypereutectic Al–23 wt.% Si alloy powder (23 Si, 2 Ni, 1 Cu, rest Al), 15–45  $\mu\text{m}$ , was selected as the matrix (Fig. 1(a)). Each powder particle contains homogeneously distributed, very fine primary Si particles throughout the  $\alpha$ -Al matrix. These Si particles precipitated out from the hypereutectic Al–Si alloy during solidification in the atomization process. Transmission electron microscopy (TEM) investigation of these prealloyed powders confirmed the presence of fine primary silicon particles of 40–100 nm size [47,48]. 10 wt.% MWCTs (95% purity, 40–70 nm diameter, 0.5–2.0  $\mu\text{m}$  length) were used as reinforcement in the synthesis of the MMC. A TEM micrograph (Fig. 1(b)) of the MWCNT shows a clean surface without amorphous carbon or any other impurity.

The composites were synthesized by two different thermal spray methods, namely plasma spray forming (PSF) and HVOF spraying. In thermal spray processes, the feedstock powder is sprayed and deposited on the substrate at a very high speed in the molten/semi-molten state [49,50]. The flame is created either by an arc in between two electrodes in the case of PSF or by the combustion of an oxy-fuel mixture during HVOF. The velocity of the particles exiting from the flame is 250–1000  $\text{m s}^{-1}$  in the case of PSF and 700–1400  $\text{m s}^{-1}$  for HVOF [49,50]. Thus, the sprayed particles experience higher heat but lower impact during PSF than in the case of HVOF spraying. Al–Si powder and MWCT were blended and mixed in a ball mill for 48 h to achieve homogeneous mixing. The powder–CNT agglomerates were sprayed on an aluminum substrate to form deposits of 0.64 and 1.25 mm by PSF and HVOF spraying, respectively. The processing and characterization details have been provided in our earlier research papers [25,26].

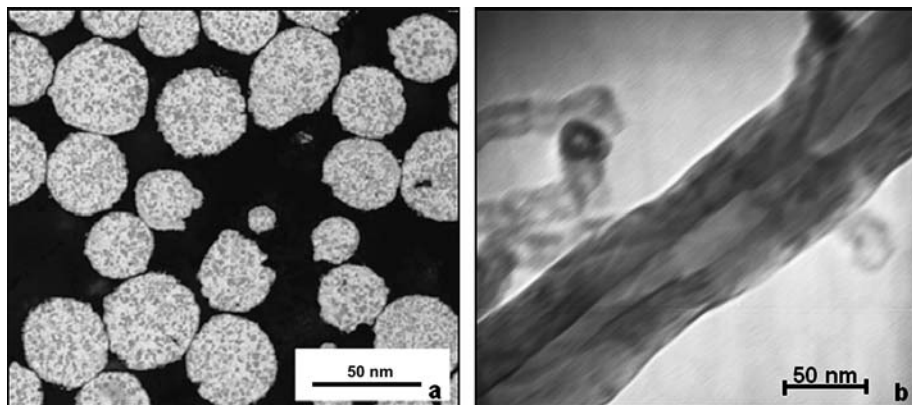


Fig. 1. (a) As received gas atomized, spherical hypereutectic Al–23 wt.% Si powder showing primary Si distributed throughout  $\alpha$ -Al and (b) as received multiwalled carbon nanotube (40–70 nm) showing impurity free surface.

## 2.2. Analytical techniques

Scanning electron microscopy of the as-received Al–Si powder and MWCNTs were carried out using a JEOL JSM-6330F field emission scanning electron microscope operated at 15 kV. The interfacial reaction product formation between the MWCNT and the Al–Si was analyzed by employing a Philips/FEI Tecnai F30 field emission transmission electron microscope at an acceleration voltage of 300 keV. First stage thinning of the sprayed deposits was carried out by metallographic polishing to 600 grit, followed by punching 3 mm diameter samples. These circular samples were then polished with a dimple grinder (Model 656 Mk3, Gatan, Inc., CA, USA). The final thinning was performed using a twin-jet polisher (Model 110, E.A. Fischione Instruments, Inc., PA, USA) along with an automatic power controller. The surface chemistry of the composites was studied by X-ray photoelectron spectroscopy (XPS) with a PHI ESCA spectrometer (Perkin–Elmer 5400), with an energy resolution of  $\pm 0.1$  eV, at a base pressure of  $5 \times 10^{-9}$  Torr, using Mg  $K_{\alpha}$  radiation (1253.6 eV). The X-ray power during the analysis was 350 W. Both the survey and the high-resolution narrow-scan spectra were recorded at pass energies of 44.75 and 35.75 eV, respectively, to achieve maximum spectral resolution. The binding energy (BE) of the Au  $4f_{7/2}$  at  $84.0 \pm 0.1$  eV was used to calibrate the BE scale of the spectrometer. Any charging shifts produced by the samples were carefully removed using a BE scale referred to C (1s) BE of the hydrocarbon part of the adventitious carbon line at 284.6 eV [51]. The peak deconvolution was done using a peak fit software with Savitsky–Golay smoothing of the data. The peak shape was fitted using Gaussian–Lorentzian mixed line shapes. The  $r^2$  value of fitting was  $\sim 0.998$ .

## 3. Results and discussion

### 3.1. Theoretical prediction of interface reaction product

#### 3.1.1. Thermodynamic consideration

Wettability is influenced by the nature of the reaction at the interface of the matrix and the reinforcement. In the case of the Al–graphite system, the contact angle is as low as  $\sim 55^\circ$ , which is attributed to the formation of aluminum carbide [35,41]. In the present case, where the Al alloy contains 23 wt.% Si, there is also a possibility of silicon carbide formation. The kinetics of carbide formation will be discussed later. The Gibbs free energy of formation for different carbide phases of aluminum and silicon as a function of temperature have been calculated and are plotted in Fig. 2 [52]. Formation of  $\beta$ -SiC is thermodynamically more feasible in hypereutectic Al–23 wt.% Si alloy than the other carbides (Fig. 2). For example, at 2000 °C the free energy of formation for  $\beta$ -SiC ( $-280 \text{ kJ mol}^{-1}$ ) is lower than that of  $\text{Al}_4\text{C}_3$  ( $-64 \text{ kJ mol}^{-1}$ ). It has been observed that the formation of  $\beta$ -SiC improves the wettability of molten Al–Si alloy on graphite surfaces [34,54].

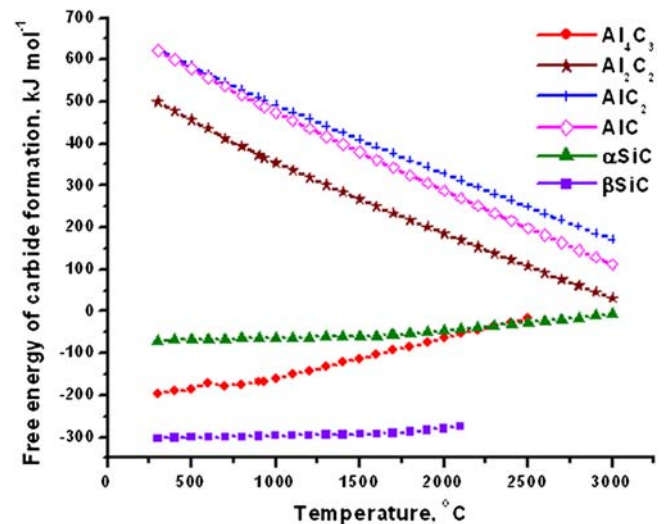


Fig. 2. Gibbs free energy of carbide formation shows feasibility of  $\beta$ -SiC formation over other carbides of silicon and aluminum.

In our present work, the Al–Si alloy is reinforced with MWCNTs rather than graphite. Carbide formation is restricted at the matrix/nanotube interface due to the absence of a prism plane in MWCNTs. The formation and the growth of carbides have been exhibited only along the reactive prism planes (100 and 110) in the graphitic structure, and these planes are absent in MWCNTs [17]. Formation of carbon nanotubes occurs by folding of the graphitic basal plane (001), and, depending on the folding plane (i.e. 100 and 110 plane), armchair and zigzag structures are formed, respectively. Prism planes are not available in carbon nanotubes of different chirality. Nevertheless, the physical damage of a few multiwalled carbon nanotubes is likely during thermal spraying at very high temperature due to the heavy impact resulting from the high spray velocity. The physical damage to the outer surface of the MWCNTs could possibly break some carbon bonds in the prism planes, where the formation of silicon carbide is feasible. The carbide formation is also possible due to the defects present in the as-received carbon nanotubes. The presence of the surface defects on the prismatic planes in the CNTs will serve as sites for functionalization via reaction with the silicon from the Al–Si matrix.

#### 3.1.2. Reactive wetting kinetics in MWCNT-reinforced Al–Si composite

According to Young's equation, where solid, liquid and vapor are in equilibrium (Eq. (1)), the wettability improves with (i) increase in the surface energy of the solid–vapor, (ii) decrease in the surface tension of the liquid matrix alloy and (iii) decrease in the solid–liquid interfacial energy [53]:

$$\cos \theta = \frac{\gamma_{SV} - \gamma_{LS}}{\gamma_{LV}}, \quad (1)$$

where ' $\theta$ ' is the wetting angle and  $\gamma_{SL}$ ,  $\gamma_{SV}$  and  $\gamma_{LV}$  are the surface energies at different interfaces. Depending upon the alloying composition of the matrix and the reaction prod-

uct, the value of the interfacial energies will vary with the wetting kinetics. Generally, the interfacial energy values for complex alloy composite systems are not readily available. However, it is experimentally possible (e.g. by the sessile drop method) to understand the wetting behavior of different alloy–reinforcement composites.

In the Al–graphite system, an initial wetting angle of 135–140° at 1190 °C, measured by the sessile drop method, has been reported by Eustathopoulos et al., which is typical of non-reactive metal–graphite systems, such as Cu–graphite or Ag–graphite [35,41]. In this case, the adhesion between the metal and the graphite is caused by Van der Waals interaction [53]. However, with the formation of Al<sub>4</sub>C<sub>3</sub> at the Al–graphite interface, the wetting surface for liquid Al changes to Al<sub>4</sub>C<sub>3</sub> and the wetting angle decreases to ~55° at 1190 °C [35,41,44–46]. It has also been reported that the contact angle for Al–20 wt.% Si alloy on graphite substrate decreases to ~40° at 1190 °C with formation of interfacial reaction product SiC [35,54]. It must be noted here that these wetting angle values are greatly influenced by the type of substrate processing, substrate roughness and the level of vacuum employed during the sessile drop experiment [55].

To achieve improved wettability of the molten Al–Si alloy on MWCNTs, the extension of the continuous silicon carbide layer on the MWCNT surface is necessary, so that the molten Al–Si experiences only carbide surface as it flows over the reinforcement. Based on the literature available on in-flight particle diagnostics during thermal spraying of metals and alloys [56], it can be safely assumed that the Al–Si alloy will be in a molten state during thermal spray forming, as the particle temperature does not exceed 2517 °C, the boiling point of pure aluminum.

The reactive wetting kinetics in the Al–Si composite with MWCNT reinforcement is shown schematically in Fig. 3. During the incipient stage of the interfacial reaction, C atoms break away from the MWCNT surface to react with liquid Al–Si [57,58]. Carbon atoms react with Si atoms to form a very thin layer of β-SiC on the MWCNT surface (Fig. 3(a)). The thermodynamic feasibility of β-SiC formation has been discussed above. At this stage, the contact angle ( $\theta_{\text{primary}}$ ) will be higher as the liquid Al–Si alloy at the triple point will be in contact with pristine MWCNT surface (Fig. 3(a)). The growth of the silicon carbide will occur in two directions: (i) lateral growth on the MWCNT surface; and (ii) growth perpendicular to the carbide layer (Fig. 4). The lateral growth will be caused by the reaction

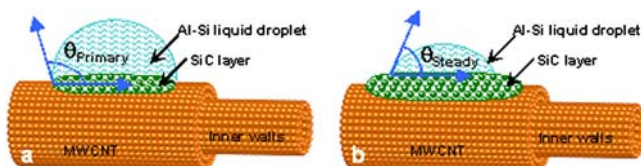


Fig. 3. Reactive wetting kinetics at MWCNT and hypereutectic Al–Si alloy, showing gradual improvement in wettability with formation of SiC layer.

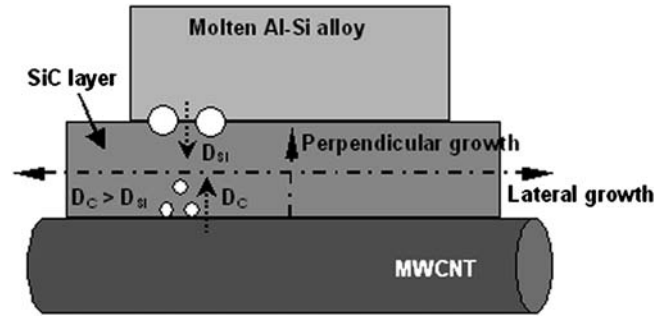


Fig. 4. Two directional growth of SiC layer between molten Al–Si alloy and multiwalled carbon nanotube reinforcement.

at the triple point, whereas the diffusion of atoms through the SiC layer will be the limiting step for perpendicular growth. The diffusion of the larger Si atoms (1.46 Å) in β-SiC crystal is only favorable by vacancy migration in regular Si sites, rather than through the tetrahedral (0.8 Å) and octahedral (1.01 Å) sites. However, the smaller C atoms (0.77 Å) can easily diffuse through the interstitial sites in the β-SiC crystal. Therefore, the activation energy required for the diffusion of C atoms is lower. The diffusivity of the C atoms ( $\sim 12.36 \times 10^{-12} \text{ cm}^2 \text{ s}^{-1}$  at 2000 °C) is approximately two orders of magnitude higher than that of Si atoms ( $\sim 8.66 \times 10^{-14} \text{ cm}^2 \text{ s}^{-1}$  at 2000 °C) through the β-SiC layer in the temperature range 2283–2547 K [57]. Thus, the perpendicular growth of the SiC layer between the liquid Al–Si matrix and the MWCNT reinforcement will occur by the diffusion of carbon atoms from the MWCNT surface to the interface of the SiC layer and the Al–Si matrix (Fig. 4). It should be mentioned here that the growth of SiC is restricted by the rapid solidification involved in thermal spraying and the available C atoms from the very stable MWCNT structure. The formation of ultrathin β-SiC (nanometer level) has been observed in TEM images (Figs. 6 and 7), as discussed later in this paper. After a critical thickness of carbide growth ( $t_{\text{crit}}$ ), the diffusion of C atoms will be negligible as the diffusion path becomes longer. Hence, the lateral growth of the carbide by the reaction at the triple point becomes prevalent and the steady-state reaction is achieved (Fig. 3(b)). In this final stage, the contact or wetting angle ( $\theta_{\text{steady}}$ ) will decrease as the Al–Si alloy flows over SiC layer (Fig. 3(b)).

The critical thickness ( $t_{\text{crit}}$ ) values for aluminum and silicon carbide layers have been calculated from Eq. (2) [42] and plotted (Fig. 5) considering the temperature dependency [51]

$$t_{\text{crit}} = -\gamma \frac{V_m}{\Delta G}, \quad (2)$$

where  $t_{\text{crit}}$  is the critical carbide layer thickness.

The energy term  $\gamma$  is calculated from the different interfacial energies of the liquid–solid–vapor system, showing reactive wetting. As the interfacial energy values are not available for the Al–Si and MWCNT system, a value of  $\gamma = 10^3 \text{ mJ m}^{-2}$  was taken to estimate the  $t_{\text{crit}}$ . This value

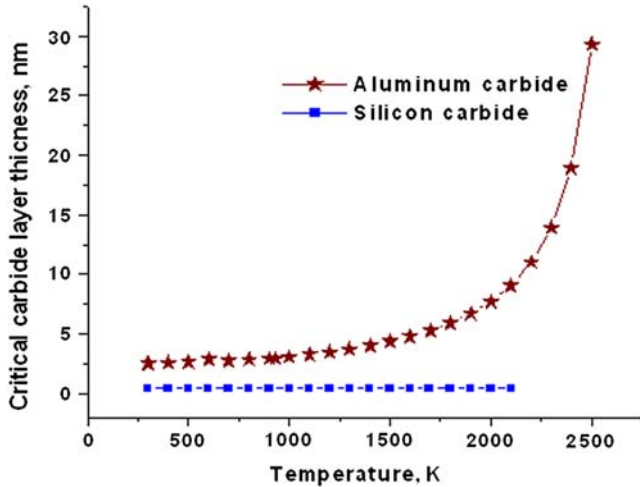


Fig. 5. Critical thickness of carbide layers for formation of SiC and  $\text{Al}_4\text{C}_3$  on MWCNT surface with respect to temperature of reaction shows lower value for SiC formation.

of  $\gamma$  is based on the available literature for the metal–Si–C system [42].  $V_m$  is the molar volume of carbides and is calculated from the density and molecular weight as  $49.56 \text{ cm}^3 \text{ mol}^{-1}$  and  $12.53 \text{ cm}^3 \text{ mol}^{-1}$  for  $\text{Al}_4\text{C}_3$  and SiC, respectively.  $\Delta G$  is the molar Gibbs free energy of the carbide formation reaction and was calculated at different temperatures, typical of those achieved during thermal spraying. It can clearly be observed from Fig. 5 that the critical layer thickness ( $\sim 0.5 \text{ nm}$ ) for SiC formation is lower than that for  $\text{Al}_4\text{C}_3$  formation ( $>2.5 \text{ nm}$ ). Thus molten Al–Si alloy will show better wettability on graphite with the formation of a silicon carbide layer.

The work of adhesion ( $W_A$ ) for different reaction products can be calculated from the Young–Dupré relation [53]

$$W_A = \gamma_{LV}(1 + \cos \theta) \quad (3)$$

$W_A$  values for spreading of aluminum on different substrates, i.e. Al–C, Al– $\text{Al}_4\text{C}_3$  and Al–SiC have been estimated by various researchers as 200, 1156 and  $1300 \text{ mJ m}^{-2}$  at 1100 K [35,43,52]. The higher values of  $W_A$  in the case of carbide formation are attributed to the covalent bonding between the C and either Al or Si in the carbide phases (as discussed by the XPS results, discussed below). Hence, a similar behavior is expected when thermally sprayed molten Al–Si alloy spreads on SiC formed due to reaction at the interface. The high work of adhesion ( $1300 \text{ mJ m}^{-2}$ ) for the Al–SiC system indicates a low contact angle. It has been observed previously that the contact angle for Al–20 wt.% Si alloy on graphite substrate decreases to  $\sim 40^\circ$  at  $1190^\circ \text{C}$  with formation of the interfacial reaction product SiC [35,54]. Although the higher work of adhesion is not a direct measurement of the improved interfacial mechanical strength, qualitatively Al–SiC interface will show better interfacial strength. The stronger interface in Al–Si composite with MWCNT reinforcement will prevent delamination and thus will improve the load transfer efficiency.

### 3.1.3. Effect of relative volume change in interfacial reaction

The relative volume change due to the formation of a reaction product at the interface also affects the wettability as the change in volume at the interface will affect the surface morphology of the substrate [59]. For example, if the volume of the interfacial reaction product is lower than that of the substrate, the substrate surface will not be completely covered by the product and will contain porosities or cavities. These volume shrinkage-induced cavities will obstruct the spreading of the liquid over the surface and result in poor wettability. The relative fractional volume change in case of formation of SiC at the interface of Si and MWCNT was calculated using Eq. (4), where  $\bar{V}_{\text{SiC}}$  ( $12.53 \text{ cm}^3 \text{ mol}^{-1}$ ) and  $\bar{V}_{\text{MWCNT}}$  ( $8\text{--}9.23 \text{ cm}^3 \text{ mol}^{-1}$ ) are the molar volumes of SiC and MWCNT

$$\text{relative volume change} = \frac{\bar{V}_{\text{SiC}} - \bar{V}_{\text{MWCNT}}}{\bar{V}_{\text{MWCNT}}} \times 100\%. \quad (4)$$

It was estimated that the volume of MWCNTs consumed during the reaction is  $\sim 40\%$  less than the volume of SiC formed. This suggests a complete coverage of the MWCNT surface by the SiC layer with no cavity or porosity at the interface. Hence, molten Al–Si alloy will experience smooth and hindrance-free spreading over this continuous SiC layer.

## 3.2. Experimental verification

### 3.2.1. SiC layer on MWCNT surface in Al–Si composite

The presence of a reaction product layer (2–5 nm) in both PSF composite and HVOF spray-formed composite is evident in Figs. 6 and 7, respectively. Based on previous thermodynamic calculations and reactive wetting kinetics in Al–Si/MWCNT composite, it is concluded that this interfacial product layer is silicon carbide. Carbide formation at the interface of multiwalled/single-walled carbon nanotubes and titanium has been reported previously by Iijima and Lee [60,61]. The formation of a 20 nm thick SiC layer at the interface of Si–MWCNT has been confirmed by Liu et al. [62]. The thickness of SiC layer in PSF composite ( $\sim 5 \text{ nm}$ ) is higher than that in the HVOF-formed composite ( $\sim 2 \text{ nm}$ ). The processing temperature in PSF is much higher than in the HVOF spraying, and this higher temperature will accelerate the diffusion of carbon atoms through SiC layer and thus promote faster growth of SiC. The extremely high heat in the plasma spraying resulted in a higher degree of melting of the Al–Si and possibly caused more breakage of carbon bonds in the MWCNT surface. Thus, more free Si and C atoms would be available to aid SiC growth. However, faster cooling rate in PSF ( $10^6\text{--}10^8 \text{ K s}^{-1}$ ) vs. that in HVOF ( $10^3\text{--}10^5 \text{ K s}^{-1}$ ) [49,50] will slow down the reaction kinetics and thus have an adverse effect on SiC growth. Our theoretical prediction suggests that the critical SiC layer thickness is 0.5 nm; however, the TEM images shows higher thickness (2–5 nm) on both PSF and HVOF-formed composites. The formation of a SiC layer  $\sim 0.5 \text{ nm}$  thick is only

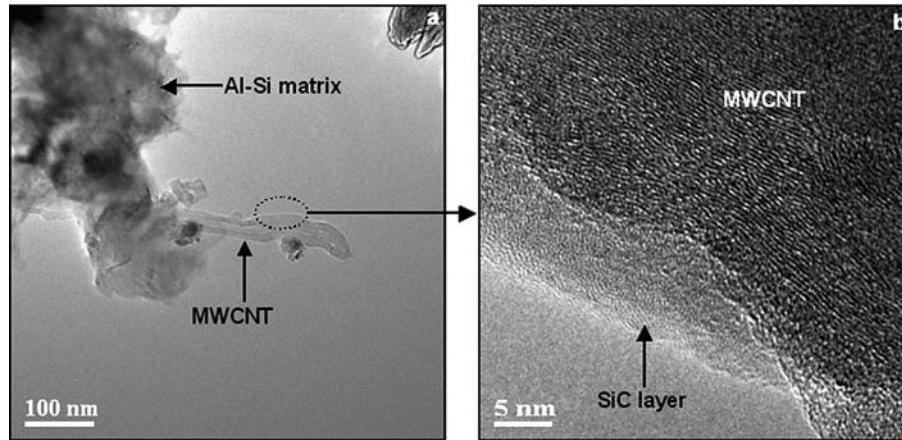


Fig. 6. Presence of silicon carbide layer ( $\sim 5$  nm) on CNT surface in plasma spray formed hypereutectic Al-Si composite reinforced with multiwalled carbon nanotube.

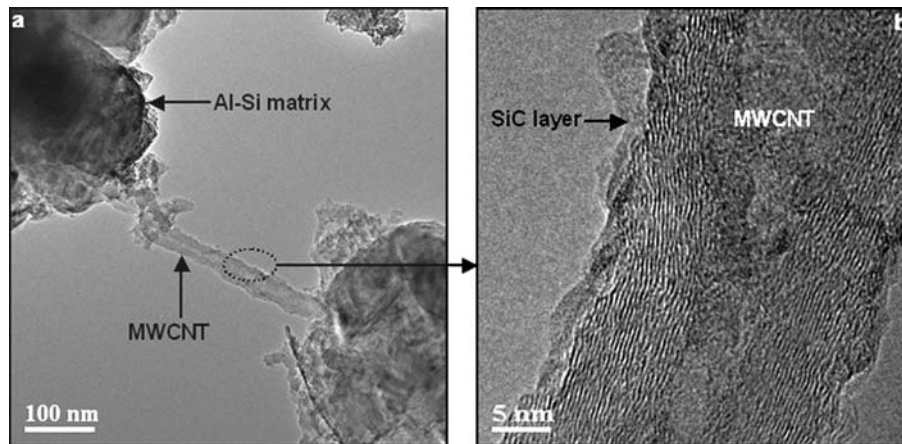


Fig. 7. Presence of silicon carbide layer ( $\sim 2$  nm) on CNT surface in high velocity oxyfuel formed hypereutectic Al-Si composite reinforced with multiwalled carbon nanotube.

possible in the case of two-dimensional monolayer SiC formation composed of  $sp^2$  bonding. However, SiC crystals tend to grow three-dimensionally because of the tetrahedral nature ( $sp^3$ ) of the Si-C bonds. The growth of the  $\beta$ -SiC crystal occurs on the (001) graphitic plane in the [111] direction, as the (001) plane in graphene sheet and the (111) plane in SiC crystal form from stacking of atoms in a hexagonal pattern [62,63]. In Figs. 5 and 6, the SiC layer on MWCNTs does not show clear crystal structure and seems to be semi-amorphous, which can be attributed to the extremely high cooling rate in thermal spray forming (PSF,  $10^6$ – $10^8$  K  $s^{-1}$ ; HVOF,  $10^3$ – $10^5$  K  $s^{-1}$ ).

### 3.2.2. Experimental verification of SiC formation on MWCNTs via Si deposition

To further confirm the formation of SiC on the MWCNT surface by the reaction of C and Si atoms, Si was deposited on as-received MWCNTs by chemical vapor deposition (CVD). Although CVD is different to thermal

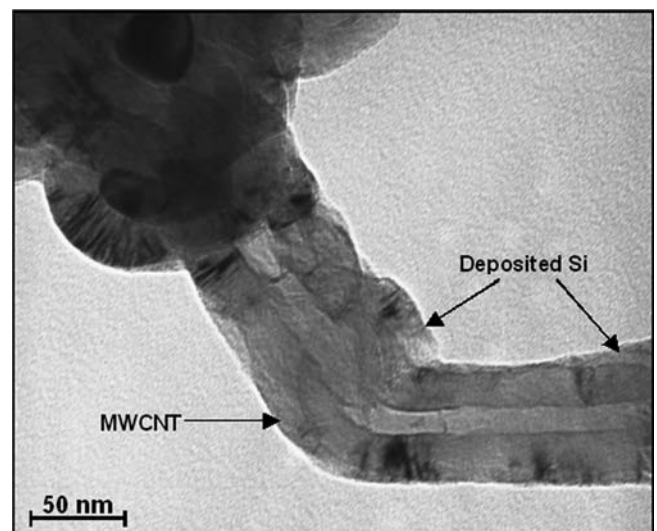


Fig. 8. Deposition of silicon on as-received MWCNT by chemical vapor deposition technique.

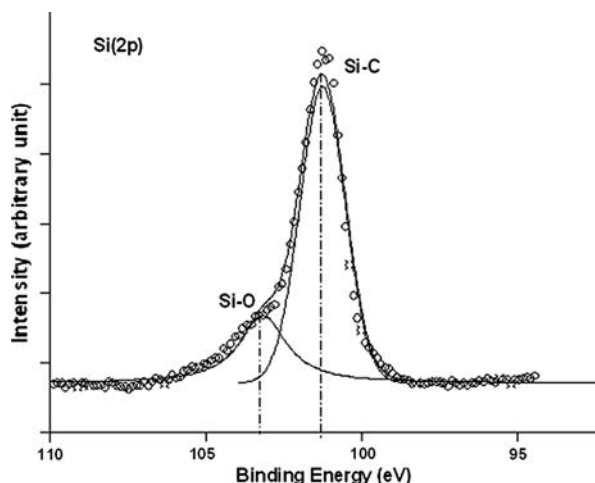
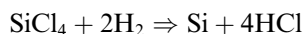


Fig. 9. Presence of Si–C bond in XPS spectrum of Si deposited MWCNT by CVD suggests the formation of SiC at the interface of Si and MWCNT.

spray processes, it can still be used as a template to study the reaction between Si atoms and MWCNTs.  $\text{SiCl}_4$  and  $\text{H}_2$  were used as reactant gases to produce Si vapor. The deposition was carried out at 1000 °C for 5 min as per the following reaction:



The TEM image of the Si-deposited MWCNTs in Fig. 8 shows a surface layer. The surface layer is not uniform and the thickness varies from 5 to 15 nm. XPS was carried out to investigate the surface chemistry on Si-deposited MWCNTs, and Fig. 9 shows the high-resolution core level Si 2p spectrum. Careful peak deconvolution with the second derivative of the spectrum reveals multiple peaks present under the single peak envelope. The peaks identified at  $101.3 \pm 0.1$  eV (full width at half maximum (FWHM) =  $1.6 \pm 0.15$  eV) and  $103.25 \pm 0.1$  eV (FWHM =  $1.64 \pm 0.15$  eV) are Si–C and Si–O type bonds. The binding energy shift was measured with reference to that of a silicon atom bound only to silicon atoms. The shift in the binding energies is attributed to the change in the Fermi level and/or change in the chemical states of the atoms. As the silicon atoms are bound to carbon atoms on the MWCNT surface, the charge transfer from the Si atoms to the more electronegative carbon peaks leads to the shifts of Si 2p peaks towards higher binding energies. The presence of the Si–O bond implies the absorption of oxygen on the surface of a SiC nanolayer with an extremely large surface to volume ratio.

#### 4. Conclusions

The wettability and the interfacial bonding influenced by interfacial reaction in a hypereutectic Al–Si composite with MWCNTs, synthesized by thermal spraying (PSF and HVOF spraying), have been studied. The formation of a  $\beta$ -SiC layer, rather than aluminum carbides at the interface of Al–Si matrix and MWCNT reinforcement, has been

confirmed theoretically and experimentally. The  $\beta$ -SiC formation at the interface of the Al–Si alloy and the MWCNT surface was restricted to an ultrathin layer (2–5 nm), attributed to the higher rate of reaction at the triple point of MWCNT/Al–Si alloy/vapor. Subsequent improvement in the wettability and the interfacial adhesion between the MWCNT reinforcement and the Al–Si matrix is suggested to be due to the formation of  $\beta$ -SiC. Both XPS and TEM analysis of Si deposited on as-received MWCNTs by CVD further confirmed the formation of  $\beta$ -SiC at the interface.

#### Acknowledgements

A. Agarwal acknowledges financial support from the National Science Foundation (NSF-DMI-0547178), and T. Laha from the Dissertation Year Fellowship by University Graduate School, Florida International University. The authors are also thankful to Plasma Processes Inc., Huntsville, AL for assistance with material processing. S. Seal further acknowledges support from the ONR YIP program.

#### References

- [1] Treacy MMJ, Ebbesen TW, Gibson JM. *Nature* 1996;381:678.
- [2] Thostenson ET, Ren Z, Chou TW. *Comput Sci Technol* 2001;61:1899.
- [3] Lu JP. *J Phy Chem Solids* 1997;58:1649.
- [4] Mamalis AG, Vogtländer LOG, Markopoulos A. *Precision Eng* 2004;28:16.
- [5] Pipes RB, Hubert P. *Compos Sci Technol* 2002;62:419.
- [6] Lau KT, Hui D. *Composites: Part B* 2002;33:263.
- [7] Mauron Ph, Emmenegger Ch, Züttel A, Nützenadel Ch, Sudan P, Schlapbach L. *Carbon* 2002;40:1339.
- [8] Desai AV, Haque MA. *Thin-Walled Struct* 2005;43:1787.
- [9] Ajayan PM, Schadler LS, Giannaris C, Rubio A. *Adv Mater* 2002;12:750.
- [10] Wong M, Paramsothy M, Xu XJ, Ren Y, Li S, Liao K. *Polymer* 2003;44:7757.
- [11] Koerner H, Price G, Pearce NA, Alexander M, Vaia RA. *Nat Mater* 2004;3:115.
- [12] Schadler LS, Giannaris SC, Ajayan PM. *Appl Phys Lett* 1998;73:3842.
- [13] Wood JR, Zhao Q, Wagner HD. *Composites: Part A* 2001;32:391.
- [14] Kymakis E, Alexandou I, Amaratunga GAJ. *Synth Met* 2002;127:59.
- [15] Szeleifer I, Yerushalmi-Rozen R. *Polymer* 2005;46:7803.
- [16] Lefrant S, Baltog I, Chappelle ML, Baibarac M, Louarn G, Journet C, et al. *Synth Met* 1999;100:13.
- [17] Kuzumaki T, Miyazawa K, Ichinose H, Ito K. *J Mater Res* 1998;13:2445.
- [18] Zhong R, Cong H, Hou P. *Carbon* 2003;41:848.
- [19] Carreño-Morelli E, Yang J, Couteau E, Hernadi K, Seo JW, Bonjour C, et al. *Phys Status Solidi* 2004;201:R53.
- [20] Kuzumaki T, Ujiie O, Ichinose H, Ito K. *Adv Eng Mater* 2000;2:416.
- [21] Dong S, Tu J, Zhang X. *Mater Sci Eng A* 2001;313:83.
- [22] Tu J, Zhu L, Chen W, Zhao X, Liu F, Zhang X. *Trans Nonfer Met Soc China* 2004;14:880.
- [23] Chen WX, Tu JP, Wang LY, Gan HY, Xu ZD, Zhang XB. *Carbon* 2003;41:215.
- [24] Chen X, Xia J, Peng J, Li W, Xie S. *Compos Sci Technol* 2000;60:30.
- [25] Laha T, Agarwal A, McKechnie T, Seal S. *Mater Sci Eng A* 2004;381:249.

- [26] Laha T, Liu Y, Agarwal A. *J Nanosci Nanotech* 2007;7:1.
- [27] Schwartz MM. *Composite materials. Processing, fabrication and application*, vol. II. Englewood Cliffs (NJ): Prentice-Hall; 1997. p. 143.
- [28] Donaldson SL, Miracle DB. *Metal handbook: composites*, vol. 21. Materials Park (OH): ASM international; 2001.
- [29] Andrews R, Weisenberger MC. *Curr Opin Solid State Mater Sci* 2004;8:31.
- [30] Asthana R. *Metal Trans A* 1994;25A:225.
- [31] Delannay F, Frozen L, Dryttere A. *J Mater Sci* 1987;22:1.
- [32] Allen KW. *Phys Tech* 1988;19:234.
- [33] Sobzak N, Stobierski L, Radziwill W, Ksiazek M, Warmuzek M. *Surf Interface Anal* 2004;36:1067.
- [34] Asthana R, Sobczak N. *JOM-e* 2000:52.
- [35] Landry K, Kalogeropoulou S, Eustathopoulos N. *Mater Sci Eng A* 1998;254:99.
- [36] Gou J, Minaie B, Wang B, Liang Z, Zhang C. *Comput Mater Sci* 2004;31:225.
- [37] Thstenson ET, Ren Z, Chou TW. *Compos Sci Technol* 2001;61:1899.
- [38] Meyer RR, Sloan J, Dunin-Borkowski RE, Kirkland AI, Novotny MC, Bailey SR, et al. *Science* 2000;289:1324.
- [39] Banerjee S, Hemraj-Benny T, Wong SS. *Adv Mater* 2005;17:17.
- [40] Bae J, Jang J, Yoon SH. *Macromol Chem Phys* 2002;203:2196.
- [41] Eustathopoulos N. *Acta Mater* 1998;46:2319.
- [42] Landry K, Rado C, Voitovich R, Eustathopoulos N. *Acta Mater* 1997;45:3079.
- [43] Landry K, Eustathopoulos N. *Acta Mater* 1996;44:3923.
- [44] Kalogeropoulou S, Rado C, Eustathopoulos N. *Scripta Mater* 1999;41:723.
- [45] Choh T, Kammel R, Oki T. *Z Mettalkde* 1987;78:286.
- [46] Landry K, Kalogeropoulou S, Eustathopoulos N, Naidich Y, Krasovsky V. *Scripta Mater* 1996;34:841.
- [47] Laha T, Agarwal A, McKechnie T, Rea K, Seal S. *Acta Mater* 2005;53:5429.
- [48] Rea K, Agarwal A, McKechnie T, Seal S. *Microsc Res Technol* 2005;66:10.
- [49] Fauchais P, Vardelle A, Dussoubs B. *J Thermal Spray Tech* 2001;1:44.
- [50] Herman H, Sampath S. In: Stern KH, editor. *Metallurgical and protective coatings*. London: Chapman & Hall; 1996. p. 261.
- [51] Barr TL, Seal S, Krezoski S, Petering DH. *Surf Interface Anal* 1996;24:99.
- [52] Kosolapova TY, editor. *Handbook of high temperature compounds: properties, production, applications*. New York: Hemisphere; 1990. p. 228.
- [53] Davies JT, Rideal EK. *Interfacial phenomena*. New York: Academic Press; 1961. p. 34.
- [54] Ip SW, Sridhar R, Toguri JM, Stephenson TF, Warner AEM. *Mater Sci Eng A* 1998;244:31.
- [55] Candan E. *Turkish J Eng Environ Sci* 2002;26:1.
- [56] Vattulainen J, Hamalainen E, Hernberg R, Vuoristo P, Mantyla T. *J Thermal Spray Tech* 2001;10:94.
- [57] Hon MH, Davis RF. *J Mater Sci* 1980;15:2073.
- [58] Favre A, Fuzellier H, Suptil J. *Ceram Int* 2003;29:235.
- [59] De Hosson JThM. In: Dahotre NB, Sudarshan TS, editors. *Intermetallic and Ceramic Coatings*. New York: Marcel Dekker; 1999. p. 307.
- [60] Zhang Y, Ichihashi T, Landree E, Nihey F, Iijima S. *Science* 1999;285:1719.
- [61] Lee JO, Park C, Kim JJ, Kim J, Park JW, Yoo KH. *J Phys D* 2000;33:1953.
- [62] Liu JW, Zhong DY, Xie FQ, Sun M, Wang EG, Liu WX. *Chem Phys Let* 2001;348:357.
- [63] Taylor A, Laidler DS. *Brit J Appl Phys* 1950;1:174.